Synthesis and Characterization of Highly Cross-Linked, Monodisperse Core−Shell and Inverted Core−Shell Colloidal Particles. Polystyrene/Poly(*tert*-butyl Acrylate) Core−Shell and Inverse Core−Shell Particles

S. Kirsch,*,† A. Doerk, E. Bartsch,* and H. Sillescu

Institute of Physical Chemistry, Johannes Gutenberg-Universitaet, Jakob-Welder-Weg 15, 55099 Mainz, Germany

K. Landfester and H. W. Spiess

Max-Planck Institute for Polymer Research, Postfach 3148, 55021 Mainz, Germany

W. Maechtle

Polymer Research Laboratory, BASF Aktiengesellschaft, 67056 Ludwigshafen, Germany

Received June 9, 1998; Revised Manuscript Received March 28, 1999

ABSTRACT: We report on the synthesis of nearly monodisperse phase-separated polymer latexes with a well-defined core−shell morphology. Styrene/diisopropenylbenzene and *tert*-butyl acrylate/ethylene glylcol-diacrylate were used for either the core or shell of the composite microgel particles. A major concern of the paper is the detailed characterization of the core−shell and inverse core−shell particles by static and dynamic light scattering, transmission electron microscopy, solid-state NMR, and the analytical ultracentrifuge. The effect of the cross-linking agent on the final phase-separated morphology is discussed and compared with theoretical predictions.

1. Introduction

Latex materials in which a core of one polymer is surrounded by a shell of a second polymer are important in many different industrial applications. This is due to the fact that, compared to materials made by blending or copolymerization, particles of such well-defined morphology have unique physical properties as different material attributes can be associated with well-defined compartments—the core and the shell. For example, those with core and shell polymers differing in their glass transition temperatures T_g may be used to modify the properties of latex-based paints.[1,2] Here, a high T_g core imparts improved mechanical stability, while the low T_g shell allows for good film-forming ability. Core−shell latexes with polymer phases differing in pH sensitivity have been made to manufacture void-containing particles that can be used as opaquifiers in coatings.[3] Two-stage latexes have potential as thermoplastic elastomers or as additives in high-impact plastics, but can also be considered as model systems to study the relationship between morphology and mechanical properties in polymer blends.[4]

Besides such technological applications, the development of core−shell particles with well-defined optical properties is of interest from more fundamental considerations as well, since they can be used to gain valuable information about the properties of highly concentrated dispersions. In particular, the dynamics in very highly concentrated dispersions has recently gained special attention, as it has been shown that colloidal particles can undergo a concentration-driven glass transition.[5−8] The dynamics close to this glass transition as monitored by dynamic light scattering show similarities to the behavior of classical atomic liquids which can be well understood within theoretical concepts.[9,10] In this context, it is of great importance to develop a colloidal host-tracer system that allows study of the single particle motion of colloidal particles interacting like "hard spheres" up to very high concentrations. The requirements for such a system are rather high. To apply light scattering techniques, the colloidal particles must have nearly the same refractive index as the solvent in order to avoid multiple scattering.[11] The dual requirement of well-defined interactions and feasibility of index matching has led to the development of highly cross-linked particles.[12] The high degree of cross-linking allows one to generate hard-sphere-like interactions[13] and imparts form stability even when using organic solvents as a dispersing medium. The choice of organic solvents, in turn, allows the refractive index matching condition (isorefractivity) for a variety of polymer materials. The main advantage of using such a system is that no adsorbed or grafted layer for steric stabilization is needed to prevent particle aggregation. Furthermore, the microgel particles can be made completely invisible by refractive index matching with a suitable solvent without the interference from a stabilization layer with a different refractive index as the main polymer. The single particle motion in the highly concentrated regime can then be monitored by adding a few tracer particles as strong scatterers, thereby simulating an optically dilute system. Core−shell microgel colloids are ideal candidates to realize optimal tracer particles. They can be designed to combine a shell made of the same material as the surrounding host colloids, to guarantee identical surface properties and, thereby, interactions, with a core that represents a strong scatterer in a solvent isorefractive to the host colloids.

* Corresponding authors.
† Present address: Polymer Research Laboratory ZKD, BASF Aktiengesellschaft, 67056 Ludwigshafen, Germany.

10.1021/ma980916e CCC: $18.00
Published on Web 06/17/1999

However, a well-defined core−shell structure is not easy to achieve, since morphological control of the synthesis has not yet been entirely understood. Although particles may be synthesized in two successive stages, a core−shell structure is not always obtained. Various alternative structures, e.g., raspberry-, confetti-, champignon-, or sandwich-like, have been described in the literature as intermediates[14] of the phase-separation process. Two main strategies to achieve advanced morphologies such as core−shell structures have to be considered. The first one is the thermodynamic stability of the formed particles. Here, the resulting two-stage particle structure can be influenced by varying the relative hydrophobicities of the monomers[15,16] (and thus the surface energies of the polymer phases). The second way of controlling particle morphology takes advantage of kinetic stability, i.e., by freezing the phase-separation process by slowing down or effectively stopping diffusion of the polymer chains during particle growth. Two different approaches can be used: (i) temperature control during reaction (i.e., changing the difference of the reaction temperature with respect to the glass transition temperature of the polymer chain) and (ii) the formation of polymer phases that are cross-linked and have a specific cross-link density (c.d.).[17] Both methods lead to an immobilization of radical-carrying oligomer components in specific regions of the growing colloidal particles. Such a strategy can be used to prepare core−shell latexes where the shell contains the more hydrophobic polymer—a situation difficult to achieve otherwise due to the mechanism of core−shell inversion described for this type of two-stage latexes.[17,18]

To gain morphological control on the synthesis of two-stage latexes requires a careful characterization of the formed particles. Different measuring techniques are available to quantitatively characterize the particle morphology and parameters such as particle radius and size distribution. They allow some conclusions to be drawn on the mechanism of particle formation as well. Static (SLS) and dynamic light scattering (DLS) are standard methods to get information about the particle size and particle size distribution.[11,19,20] The method of analytical ultracentrifugation (AUC)[21] is a powerful tool to fractionate a sample of latexes in order to obtain the full shape of various distribution functions such as the molecular weight distribution (MWD), the particle size distribution (PSD), and the density distribution (DD).[21] Small-angle X-ray[22,23] and small-angle neutron scattering[24] have been used to gain detailed information on the particle morphology of core−shell particles. Solid-state NMR spectroscopy[25] has been recently established as a new and powerful method to study the internal structure of phase separated polymer components. Related works on this topic are studies of domain structures in diblock copolymer systems[26] and experiments on core−shell latexes,[27,28] where the method of ^{1}H spin diffusion was used.

The core−shell particles whose synthesis is reported are tailor-made to be colloidal tracer particles in a host-tracer system. Highly cross-linked poly(*tert*-butyl acrylate) microgel colloids were used up to high concentrations as host particles using 4-fluoro-toluene as an isorefractive solvent. Our study of the collective and single particle dynamics of those highly concentrated colloidal dispersions will be presented elsewhere.[29] Here, we will focus on the detailed analysis of the morphology of the core−shell particles. The synthesis of the seed latexes will be presented in a forthcoming publication.[30]

The paper is organized as follows: In section 2 the experimental details of the synthesis of the phase-separated core−shell latexes are given. Then, in section 3, the characterization of the colloids by transmission electron microscopy, differential scanning calorimetry, light scattering techniques, the analytical ultracentrifuge, and solid-state nuclear magnetic resonance is reported. In section 4 the results obtained for the core−shell structured particles are discussed.

2. Experimental Section

2.1. Materials. Styrene (S) and *tert*-butyl acrylate (TBA) from Aldrich were distilled three times under N_2 reduced pressure before use. 1,3-Diisopropenyl benzene (DIPB) (Fluka) and ethylene glycol diacrylate (EGDA) (Aldrich), used as cross-linking monomers, were treated in the same way. The initiator $K_2S_2O_8$ (KPS) (Aldrich) and the emulsifier sodium dodecyl sulfate (SDS) (Serva Chemie) were used without further purification. Deionized, bidistilled water was used during all polymerization processes after filtration through a low-pressure ultrafiltration unit (Berghof, filter from Schleicher & Schuell with 0.1 μm pore size).

All polymerizations were carried out in a 500-mL three-necked flask fitted with a reflux condensor, a microfeeder, a T-shaped PTFE/glass stirrer, and N_2 gas inlet. The stirring speed was 350 rpm for all reactions. The reaction temperature was 343 K in all preparations.

2.2. Preparation of Core−Shell Particles under Semicontinuous Reaction Conditions. 2.2.1. Synthesis of Particles with a Quasi Core−Shell Structure (SK-25). Seed latexes were prepared as described in ref 30. Samples of 0.125 mol of TBA, 6.24 mmol of EGDA, 350 mL of water, and 0.304 mmol of KPS dissolved in 30 mL of water were used. The shell layer was built by swelling the seed latex with a mixture of 6.9 mmol of TBA/0.682 mmol of EGDA for 1 h. Then the reaction was started by adding 0.304 mmol of KPS dissolved in 30 mL of water. By use of a microfeeder another mixture of 0.04 mol of TBA/3.99 mmol of EGDA was added during 1 h. The reaction time for both layers was 24 h to ensure high conversion.

2.2.2. Synthesis of highly Cross-linked PS core, PTBA shell particles (SK-26). The PS core/PTBA shell latexes (SK-26) were synthesized in a two-step polymerization. The PS microgel seed particles were prepared in analogy to Kotera et al.[31] In a variation of the recipe in ref 31 a certain amount of cross-linker as comonomer was used to form microgel particles. For this reaction, 0.052 mol of S with 2.58 mmol of DIPB in 360 mL of water were placed into a 500-mL flask and the reaction was initiated by adding 0.481 mmol of KPS dissolved in 30 mL of water. The reaction time for the PS microgels was 48 h. For the preparation of the PTBA/EGDA shell, a mixture of 7.81 mmol of TBA/0.39 mmol of EGDA was swollen into the seed particles for 1 h. Again, the reaction is started by adding 0.48 mmol of KPS dissolved in 20 mL water. For particle growth, a mixture of 0.032 mol of TBA with 1.6 mmol of EGDA was added within 1.5 h using a microfeeder, leading to a 1:10 cross-linked shell.

2.2.3. Synthesis of highly Cross-linked PTBA core, PS shell latexes (SK-27). Due to its stronger hydrophobic character, the PS phase is unlikely to form the surface of a PTBA/PS core−shell structure, even if added to a preformed PTBA seed. Instead, one would expect a phase inversion via polymer diffusion,[17,18] leading to a thermodynamically more stable domain or even PS/PTBA core−shell structures. Thus, to achieve such a PTBA/PS core−shell morphology, henceforth denoted as "inverse core-shell" (ICS) structure (SK-27), a three-step polymerization process was adopted. The strategy underlying this three-stage procedure will be discussed in section 4.

The PTBA seed particles were prepared in the same manner as the particles described in ref 30. The overall reaction conditions were identical to those described in section 2.2.2.

For the SK-27 ICS particles a mixture of 0.125 mol of TBA and 1.664 mmol of EGDA in 370 mL water was used, yielding a cross-link density of 1:50 for the seed. The reaction was started by 0.304 mmol of KPS dissolved in 30 mL of water, and the polymerization was allowed to proceed for another 24 h. The first shell layer was formed by a mixture of 0.047 mol of TBA and 7.84 mmol of EGDA (c.d. 1:5). At the beginning of the second stage, 1 g of the above mixture was added to the seed and allowed to swell it for 1 h before the reaction was started by adding 0.22 mmol of KPS dissolved in 20 mL of water. The rest of the mixture was added within 2 h. The polymerization then takes place for another 24 h. In the third stage of reaction the PS/DIPB (c.d. 1:10) shell was synthesized. The initiator (0.37 mmol of KPS dissolved in 20 mL water) was added first. Then a mixture of 0.154 mol of S and 7.71 mmol of DIPB was added within 3 h. The reaction time for the last stage was 24 h.

2.3. Characterization Methods. 2.3.1. Transmission Electron Microscopy (TEM). The TEM measurements were performed using a Zeiss EM 902 microscope at an accelerator voltage of 80 keV. All samples were prepared from filtered, 1:100 diluted emulsions and dried on a slide for 30 min. Then the latexes were coated by a carbon film.

2.3.2. Light Scattering. All light scattering experiments were performed with an ALV 5000 correlator from ALV, Langen, and a self-made optical setup[8] with a Ne−YAG solid-state ring laser unit (DPSS-50; Coherent), emitting 50 mW in the TEM_{00} CW mode at a wavelength of $\lambda = 532$ nm. Measurements were performed in emulsion as well as in organic solvents. Dynamic light scattering[11,32] (scattering angle $2\vartheta = 90°$; $q = (4\pi n_D/\lambda) \sin \vartheta$; n_D = refractive index of dispersing medium) was used to obtain the hydrodynamic radius $R_H = \langle R^6\rangle/\langle R^5\rangle$, where $\langle R^n\rangle$ denotes the nth moment of the particle size distribution. With the same setup the particle form factor $P(q)$ of the latexes was determined via static light scattering[19] (100 s per scattering angle). From the location of the minima in $P(q)$ the mean radius $\langle R\rangle$ was obtained via the relation[20] $q\langle R\rangle = 4.49, 7.73, ...$ To gain information on the width of the particle size distribution (PSD), i.e., the polydispersity $\sigma = (\langle R^2\rangle - \langle R\rangle^2)^{1/2}/\langle R\rangle$, the region around the first minimum of $P(q)$ was fitted with an analytical relation which essentially corresponds to averaging the $P(q)$ of a homogeneous sphere over a Schultz distribution of particles sizes according to[20]

$$I(q) \propto \int_0^\infty G(R)\, P(qR)\, R^6\, \mathrm{d}R \qquad (1)$$

In an analogous manner, σ can be obtained via the q dependence of the diffusion coefficient in dilute dispersion that arises at q values around the first minimum in $P(q)$ according to[20]

$$D_0(q) = \frac{\int_0^\infty G(R)\, P(qR)\, D_0(R)\, R^6\, \mathrm{d}R}{I(q)} \qquad (2)$$

It should be noted that this type of analysis requires that at least one minimum of $P(q)$ falls into the accessible angular range of the light scattering setup. This limits its application to particles larger than about 150 nm in radius.

2.3.3. Analytical Ultracentrifugation (AUC). All measurements were performed in an eight-cell AUC setup (a modified Spinco-Beckman AUC, Model E, Palo Alto, CA; see refs 21 and 34) and in a homemade AUC-particle sizer, described in ref 35. Two samples were measured: the PS core dispersion SK-26 and the PS/PTBA core−shell dispersion SK-26. The latter sample was studied in aqueous dispersion as well as in organic solvents.

2.3.4. Nuclear Magnetic Resonance (NMR). ^{1}H spectra were recorded on a Bruker MSL-300 NMR spectrometer equipped with a standard Bruker MAS probe head. All samples were spun at frequencies of 3 kHz. The 90°-pulse lengths were in the range of 3.5−4.0 μs. The ^{1}H spin diffusion experiments were carried out with selection of the soft component PTBA using the dipolar filter. One filter cycle consists of a pulse sequence of 12 ^{1}H 90° pulses separated by a delay time t_d of 10 μs and can be repeated 1−20 times. Typically, 100−200 scans of the ^{1}H spectra were accumulated with a repetition time of 2 s. The measuring time for a ^{1}H spectrum was about 5 min.

3. Results

3.1. Transmission Electron Microscopy. In Figure 1 transmission electron microscopy (TEM) pictures of the PTBA quasi core−shell particles (SK-25, Figure 1a,b), the PS/PTBA core−shell (SK-26, Figure 1c,d), and the PTBA/PS inverse core−shell (SK-27, Figure 1e,f) latexes are shown with different magnifications.

In the TEM picture of the SK-25 latexes most of the colloidal particles are damaged by the electron beam. Only a few of them show the original size and shape (Figure 1b). Therefore, only indirect methods such as light scattering measurements or analytical ultracentrifugation, presented in the following sections, give information on particle size and size distribution. Similar destruction of the PTBA by the electron beam is visible in the TEM pictures of the PS/PTBA core−shell latexes (SK-26) given in Figure 1c,d. Most of the particles are covered by a closed film formed from the shell material of several particles. Nevertheless, there exist regions in the electron micrograph where the core−shell morphology is clearly visible. Such a region is depicted in Figure 1c, showing PS cores with high contrast (dark) surrounded by halos of weaker contrast (lighter shaded areas) formed by PTBA shells or their remnants. No domain structures can be detected in any of the polymer phases, indicating the existence of sharp interfaces. This is brought out more clearly in the magnification, Figure 1d. One sees a PS core without any inclusions of PTBA domains. The shell material has been melted down by the electron beam and forms a transparent film surrounding the PS core. Again, the degradation of the PTBA impedes the use of TEM for particle sizing. The TEM pictures in Figure 1e,f show particles of the sample with PTBA in the inner phase and PS as shell material (SK-27). As expected for particles with a PS surface, the particles are stable under the influence of the electron beam and show a high contrast in the shell. A nice side effect of the small shell thickness of about 20 nm is that the inner core material with its lower contrast is visible as a bright patch. No domain formation can be seen in the inner core area, and a sharp interface separates the two polymer phases. Here, particle sizing via TEM is possible. The analysis of the individual particles yields a Gaussian particle size distribution (PSD) with a standard deviation of about 7%. Thus, the reaction conditions (section 2.2.3) lead to a very small polydispersity.

3.2. Light Scattering Experiments. When analyzing static light scattering experiments on core−shell latexes consisting of different polymer materials, the contrast $\Delta n_D = n_{D,polymer} - n_{D,solvent}$ is of key importance for the interpretation of the data. It determines the scattering amplitude and, thus, the strength of the contribution of a given material to the overall scattered intensity. In water, the refractive index difference Δn_D for either PS or PTBA is sufficiently large. Thus, core and shell of the PS/PTBA or PTBA/PS particles contribute to the static scattering intensity and the experiment will reflect the particle form factor $P(q)$ of the whole, unswollen core−shell latexes. From a comparison with the $P(q)$ of the pure cores (the seed latexes) in aqeous dispersion, the first evidence for the successful

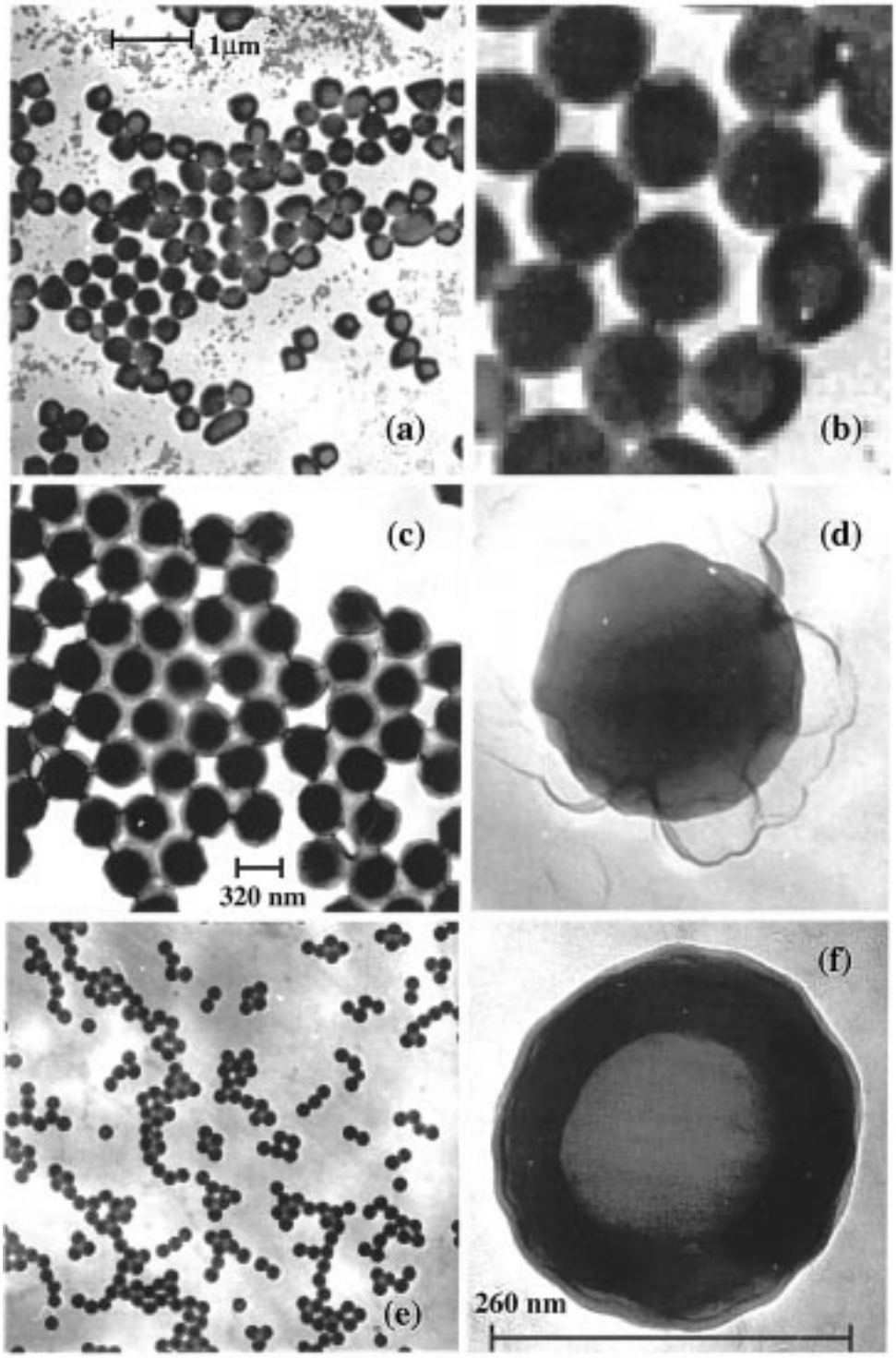

Figure 1. (a, b) TEM pictures of the quasi core−shell (SK-25) structure, see section 2.2.1. (c, d) TEM pictures of the PS/PTBA core−shell particles (SK-27), see section 2.2.2. (e, f) TEM pictures from the PTBA/PS inverse core−shell particles (SK-28), see section 2.2.3. Note the plotted scales are only drawn to allow illustration of the particle sizes.

polymerization of a shell layer around the seed latex is gained. A direct verification of the core−shell morphology is possible by measurements of $P(q)$ in the swollen state, using good solvents with different refractive indices. Here, solvents which are isorefractive to either PS or PTBA are of special interest (see below). This procedure is, in principle, very similar to the contrast variation technique used in small-angle X-ray scattering (SAXS) experiments on core−shell latexes of smaller size than studied here.[22] The main difference is that in SLS the refractive index takes up the role of the electron density in SAXS for determining the contrast. In combination with DLS measurements, which always yield the total size of the core−shell particles as they monitor the hydrodynamic radius via the particle diffusion, a detailed determination of the internal structure of the core−shell latexes is possible as will be demonstrated in the following. All results obtained by using SLS and DLS techniques for the different core−shell type particles are summarized in Table 1.

For the much simpler case of SK-25, where core and shell consist both of PTBA and differ only with respect

Table 1. Particle Size and Size Polydispersities Obtained by Light Scattering[a]

	DLS R_H/nm			SLS $\langle R \rangle$ /nm				
latex	aq dispersion	THF	4-FT	aq dispersion	THF	4-FT	2-EN	σ
SK-25								
c	–	–	–	157	–	–	–	0.07
c + s	163	291	–	167	285	–	–	
SK-26								
c	133	–	–	–	–	–	–	0.07
c + s	170	298	272	172	–	162	–	
SK-28								
c	98	–	–	–	–	–	–	0.06
c + s1	109	–	–	–	–	–	–	
c + s2	130	242	239	–	–	–	153	

[a] Dispersion media: tetrahydrofuran (THF), 4 fluorotoluene (4-FT), and 2-ethylnaphthalene (2-EN). $R_H = \langle R^6 \rangle / \langle R^5 \rangle$ denotes the hydrodynamic radii obtained from DLS. $\langle R \rangle$ (first moment of the size distribution) and size polydispersity $\sigma = (\langle R^2 \rangle - \langle R \rangle^2)^{1/2} / \langle R \rangle$ as determined from the particle form factors $P(q)$ measured by SLS. If the particle size is smaller than 150 nm, no $P(q)$ can be analyzed (see text) and the size polydispersity is estimated from cumulant analysis. The abbreviations c and s are for core and shell, respectively.

to the cross-linking density, a comparison of the radii of the core−shell particles and the corresponding seeds determined from SLS in aqueous dispersion yields a thickness of 10 nm for the second PTBA layer (cf. Table 1). Using the hydrodynamic radii of the particles obtained in aqueous dispersion and the good solvent tetrahydrofuran (THF), the swelling ratio $S = R_{swollen}^3 / R_{unswollen}^3$ can be calculated. The value $S = 5.7$ corresponds to that found for purely 1:10 cross-linked PTBA latexes ($S = 5.4$; ref 30). Thus the polymerization of a 10-nm shell of 1:5 cross-linked PTBA ($S = 2$; ref 30) is not sufficient to withstand the swelling tendency of the core.

Figure 2 shows the SLS results for the SK-26 PS/PTBA core−shell and the SK-27 PTBA/PS inverse core−shell structured particles. Figure 2a compares the $P(q)$ of the PS/PTBA latexes (SK-26) in aqueous dispersion with that in the good solvent 4-fluorotoluene (4-FT; $n_D = 1.4688$). Most strikingly, the minimum of $P(q)$ is shifted to larger q values when going from aqueous dispersion to 4-FT. This implies that the particle size in 4-FT (swollen) is smaller than that in aqueous dispersion (unswollen), a result which can immediately be understood if one takes into account that 4-FT is isorefractive to PTBA ($n_D = 1.468$). Thus, in 4-FT PTBA does not contribute to $P(q)$ and what one really measures is the size of the swollen PS cores. The swelling ratio $S = 1.8$ calculated by comparison with the unswollen core radius, as determined by DLS on the aqueous dispersion of the seed latex (cf. Table 1), is consistent with the value characteristic for 1:10 cross-linked PS latexes ($S = 2.2$; ref 30). This indicates that the swelling of the PS core is not affected by the PTBA shell, yielding indirect evidence for the existence of a sharp interface between the two polymer phases.

The knowledge of the core radius $R_H^c = 133$ nm and the thickness of the shell $d = R_H^{c+s} - R_H^c = 37$ nm in aqueous dispersion and of the corresponding values in the swollen state ($R_{4-FT}^{c+s} = 162$ nm; $d = R_{H,THF}^{c+s} - R_{4-FT}^c = 136$ nm) allows the calculation of the volume swelling of the shell, where it was assumed that PS swells similarly in 4-FT and THF.[36] The resulting value of $S = 6.2$ compares reasonably with the value for pure 1:10 cross-linked PTBA latexes ($S = 5.4$; ref 30). Analyzing the measured $P(q)$ according to eq 1 (solid lines in Figure 2a), a size polydispersity of 9 and 7% is obtained for aqueous dispersion and 4-FT, respectively. $P(q)$ data are affected by multiple scattering effects and by deviations from the Rayleigh−Debye−Gans approximation (which assumes that $\langle R \rangle < \lambda/20$ or $n_{D,latex} \approx n_{D,solvent}$; cf. ref 37) most strongly at the position of the minimum. As this leads to an overestimation of the actual polydispersities, the determined values have to be considered as upper limits.

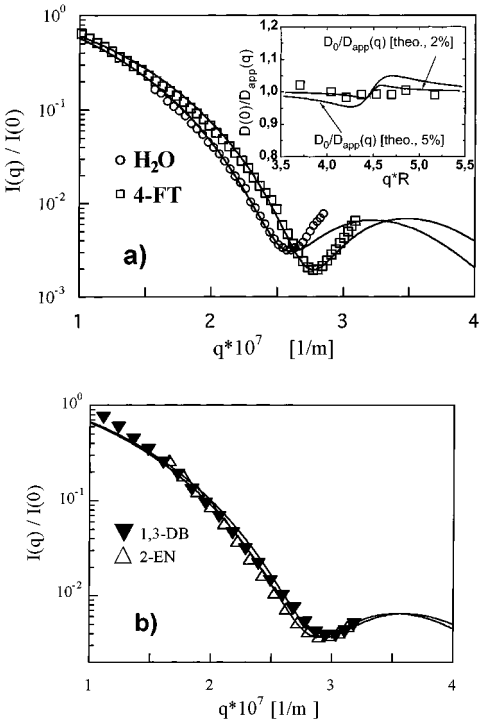

Figure 2. Results from light scattering experiments (cf. Table 1) of dilute samples of SK-26 PS/PTBA (a) and PTBA/PS (b). (a) SK-26 PS/PTBA core−shell latexes in emulsion (○, $\langle R \rangle$ = 172 nm, $\sigma = 0.09$) and 4-FT (□, $\langle R \rangle = 162$ nm, $\sigma = 0.07$). The main diagram shows the measured particle form factor $P(q)$ fitted with theoretical relation eq 1 (lines). The inset shows the q dependence of the apparent diffusion coefficient $D_{app}(q)$ in 4-FT normalized to the free particle diffusion coefficient D_0 ($R_H = 272$ nm) obtained at low wave vectors, in comparison to theory (lines), eq 2, for 2 and 5% polydispersity. (b) SK-28 in 1,3-dibromobenzene (▲, $\langle R \rangle = 152$ nm, $\sigma = 0.07$) and 2-ethylnaphthalene (△, $\langle R \rangle = 153$ nm, $\sigma = 0.1$). The lines are theoretical calculations of $P(q)$ for homogeneous scatterers, eq 1.

That the PSD is narrower than suggested from the analysis of the SLS data is indicated by the nearly q-independent diffusion coefficients in 4-FT. As indicated in the inset of Figure 2a, where the experimental data are compared with calculations according to eq 2,

only polydispersities less than 5% are consistent with the DLS results.

The PTBA/PS core−shell particles (SK-27) can be dissolved in two different good solvents which are nearly isorefractive to the PS shell ($n_D = 1.598$), i.e., 2-ethylnaphthalene (2-EN; $n_D = 1.5984$) and 1,3-dibromobenzene (1,3-DB; $n_D = 1.6080$). The results of the SLS measurements (Figure 2b) can be interpreted in a similar manner as the SK-26 PS/PTBA latexes (cf. Table 1). As a result, a volume swelling ratio of $S = 2.8$ is obtained for the core with a cross-link density of 1:50, which is much less than $S = 13.5$ obtained by swelling a pure 1:50 cross-linked PTBA/EGDA particle[30] in THF. In contrast to the SK-26 core−shell particles, the volume swelling of the core material is hindered by the highly cross-linked shell layers. Identical results of the SLS measurements are obtained for the different organic solvents (2-EN, 1,3-DBB). SLS measurements in aqueous dispersion are not useful here, due to the limitation in q discussed above. A calculation of the volume swelling ratio for the PS shell using the hydrodynamic radius of the latexes measured in THF together with the radii of the swollen cores in 2-EN and 1,3-DBB yields an anomalously high value of $S = 11$ instead of $S = 2$ for pure 1:10 cross-linked PS. Since $S = 2$ corresponds to a hydrodynamic radius of 175 nm, the discrepancy is well outside experimental error and is not understood at present. It is, however, not restricted to THF as solvent as the identical radius was found in 4-FT as well. One possible explanation would be the preferential accumulation of the cross-linker DIPB at the PTBA/PS interface which could lead to a less effective cross-linking in the outer shell. A conclusive interpretation, however, requires further systematic studies.

It should be noted that the presented analysis uses the analytical form of $P(qR)$ for homogeneous spheres. In the case of core−shell particles this is strictly correct only when the shell does not contribute to $P(q)$, i.e., when a solvent isorefractive to the shell material is used. In all other cases $P(qR)$ is more complicated, due to a discrete step in the refractive index profile. However, since no analytical solutions of eqs 1 and 2 for a polydisperse core−shell structure are available at present, we used the homogeneous sphere solution for $P(qR)$ in the other cases as well as a first approximation. We believe that the qualitative interpretation of our results is not affected by this approximation as we expect only small changes in the absolute values of the determined quantities. This will be substantiated by future work where core and shell polydispersities will be taken into account explicitly.

3.3. Analytical Ultracentrifugation (AUC). AUC measurements were performed on the SK-26 PS/PTBA core−shell particles only. In the first experiments both the core−shell particles and the corresponding seeds were analyzed in *aqueous* media. These measurements yield the particle size distribution (PSD) according to ref 38 and the average particle density ρ and the particle density distribution (i.e., the chemical heterogeneity) using density-gradient (DG) runs. In further AUC experiments both samples were transferred into *organic media* (THF and 4-FT, both representing good solvents for PS and PTBA). The degree of volume swelling S of the microgel particles can be measured by using sedimentation and density runs (see ref 39).

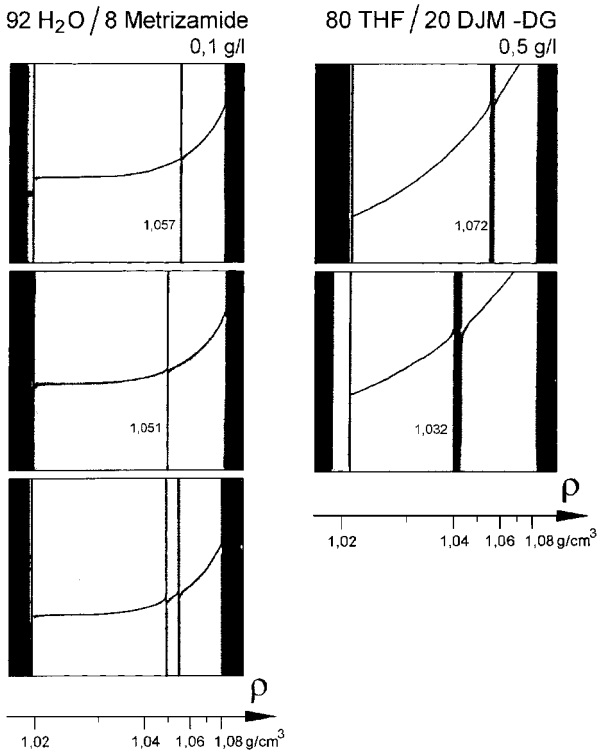

Figure 3. Schlieren photos of aqueous 92 H_2O/8 metrizamide density gradient (DG) runs of PS core particles, core−shell particles, and a 1:1 mixture of both shown as narrow turbidity bands on the left side. The two Schlieren photos on the right-hand side show the analogous turbidity bands of the first two samples in a organic solvent mixture (80% THF and 20% DIM) DG run. The resulting values for the particle densities are given in the figure.

3.3.1. AUC Measurements in Aqueous Media. The left side of Figure 3 shows three Schlieren photos of DG runs of the PS core particles, the core−shell particles, and a 1:1 mixture of both (from top to bottom) in a mixture consisting 92 parts (w/w) H_2O and 8 parts metrizamide. All pictures show very narrow DG turbidity bands, implying completely uniform particle densities and, thus, completely uniform chemical composition. This is self-evident for the PS core particles. For the core−shell particle this result implies a constant core-to-shell ratio for each particle. A distribution in the core/shell composition would result in a broad DG turbidity band. The particle density values of the two samples, following from the radial band position in the DG photo of Figure 3, are $\rho = 1.057$ and 1.051 g/cm^3 for the PS core and the PS/PTBA core−shell particles, respectively. The first value is well-known for PS latexes, and the second one is higher than the value of pure PTBA (1.029 g/cm^3) but smaller than the density value for PS as expected for a PS/PTBA core−shell particle. A calculation of the average density of the core−shell latex using the light scattering results (assuming core/shell volume additivity) yields $\rho = 1.049$ g/cm^3 which—given the experimental uncertainties of light scattering—compares favorably to the AUC result.

Figure 4a shows sedimentation runs with the AUC-turbidity detector[21] yielding the light intensity (I)−running time (t) fractionation curves of the two latexes. Both deliver very narrow single-step $I(t)$ curves, indicating a very narrow unimodal PSD. The sedimentation velocities are $s = 2200$ and 3830 svedberg units (sved) for the PS core and the core−shell particles, respectively. From these s values one obtains with Stokes law

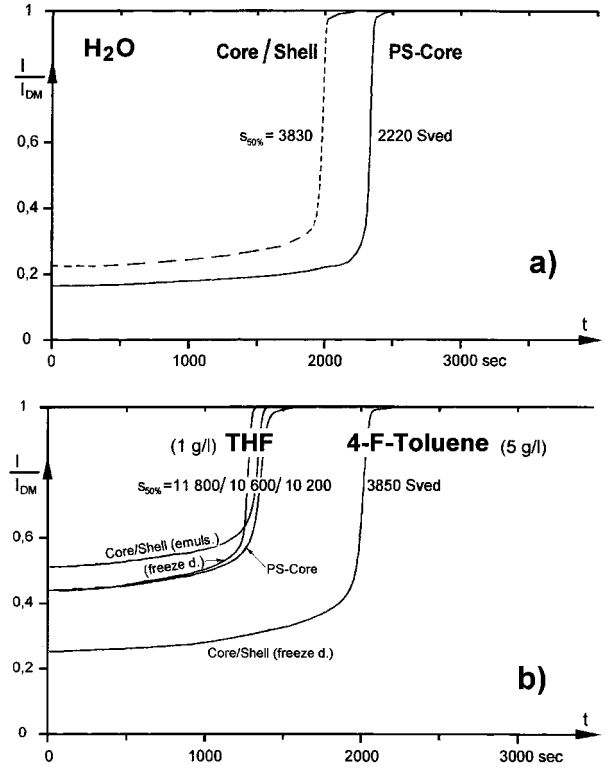

Figure 4. Sedimentation runs with the AUC-turbidity detector which yields the normalized light intensity I/I_{DM}−running time t fractionation curves of the two latexes (I_{DM}, intensity of the dispersing media). Results for PS core and PS/PTBA core−shell of the sample SK-26 in aqueous dispersion (a) and in organic solvents THF and 4-FT (b).

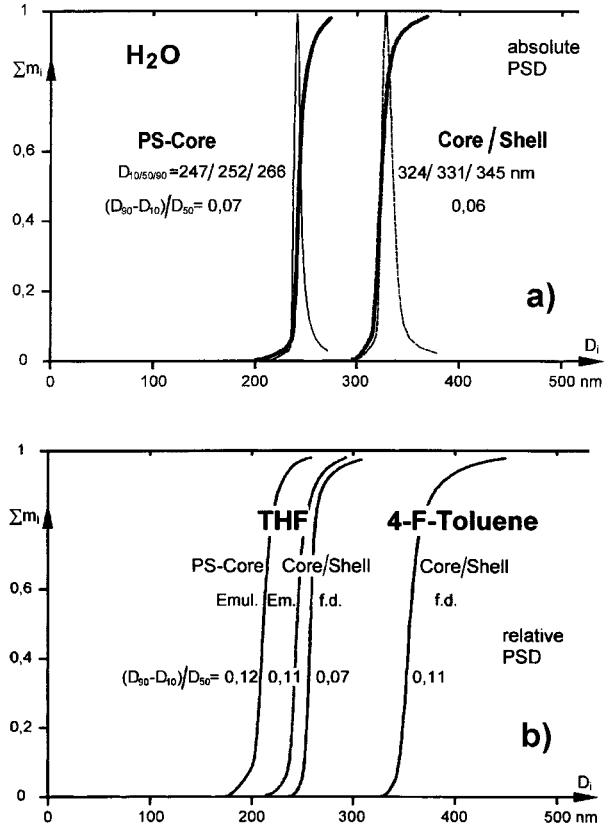

Figure 5. Calculated AUC particle size distributions from the $I(t)$ fractionation curves shown in Figure 4, for the SK-26 PS core and PS/PTBA core−shell particles in aqueous dispersion (a) as well as in THF and 4-FT (b). The PSD in (a) are absolute ones, in (b) relative ones.

particle diameters $D = [18\eta_{H_2O}s/(\rho - \rho_{H_2O})]^{1/2} = 252$ and 331 nm. With Stokes law and Mie's light scattering theory the $I(t)$ curves of Figure 4a can be transferred into the absolute PSD curves of Figure 5a, using the measured particle densities. The three characteristic diameters of every PSD are $D_{10/50/90\%} = 247/252/266$ nm (PS core) and 324/331/345 nm (core−shell), and the width of the PSD is characterized by $(D_{90\%} - D_{10\%})/D_{50\%} = 0.07$ and 0.06 for PS core and PS/PTBA core−shell particles, respectively.[40] These results imply (i) the size increase from seed latex radius to core−shell particle radius seen in the AUC measurements is consistent with the light scattering data and (ii) both samples have a uniform, narrow, and nearly monodisperse PSD, its width comparing well with corresponding light scattering data (cf. Table 1).

3.3.2. AUC Measurements in Organic Media. The right-hand side of Figure 3 shows two Schlieren photos of DG runs in THF/diiodomethane (DIM). As in the aqueous DG run (left side of Figure 3) narrow turbidity bands of big particles (Mie scatterers with $D > 200$ nm) can be detected.[41] A double Schlieren peak of dissolved linear PS or PTBA macromolecules cannot be observed. Thus, all PS core and PS/PTBA core−shell particles are completely cross-linked, giving rise to microgel particles only. Due to the narrowness and high turbidity of their DG bands, the degree of cross-linking of these microgel particles must be high and their swelling degree with THF/DIM is low.

The particle density values obtained from the THF/DIM−DG photos in Figure 3b are $\rho = 1.072$ (PS core) and 1.032 g/cm^3 (PS/PTBA core−shell). These values are only apparent ones, due to the different preferential solvation of either PS or PTBA with THF ($\rho = 0.8833$ g/cm^3) and DIM ($\rho = 3.170$ g/cm^3) inside the swollen microgel particles. Thus a calculation of an absolute PSD from the corresponding $I(t)$ fractionation curves in Figure 4b is impossible in these organic media and the PSD values in Figure 5b are only relative ones.

Figure 6 shows Schlieren photos of sedimentation runs of the PS/PTBA core−shell sample in THF and 4-FT prepared by dilution of the aqueous dispersion with organic solvent or by redispersion of the freeze-dried powder (concentrations 1 and 5 g/L, respectively), as indicated in the figure. Again, no slow Schlieren peaks of dissolved macromolecules are detectable. Instead, only fast sedimenting turbidity fronts of highly cross-linked, turbid microgel particles are seen. The sedimentation velocities of the (smallest and slowest) microgel particles from the analysis of the Schlieren photos are $s = 8200$ (core, THF), 8900/9500 (core−shell, THF) and 3000 sved (core−shell, 4-FT), as indicated in Figure 6 (the lower s values in H_2O are also included for comparison). For a more precise determination of these s values, the sedimentation run experiments shown in Figure 6 (done with the Schlieren optics detector) were repeated with the turbidity detector. The resulting four $I(t)$ curves are shown in Figure 4b. Compared to the experiments with the aqueous dispersion (Figure 4a), again very narrow single-step $I(t)$ curves are detected for all microgel dispersions in THF and 4-FT. This indicates that the PSD of the swollen microgel particles is unimodal and very narrow as well. The s values of the 50% points are: $s_{50\%} = 10\,200$ (core, THF), 10 600/11 800 (core−shell, THF), and 3850 (core−shell, 4-FT) sved. These 50% (average) values are more precise and show a higher value as compared to the

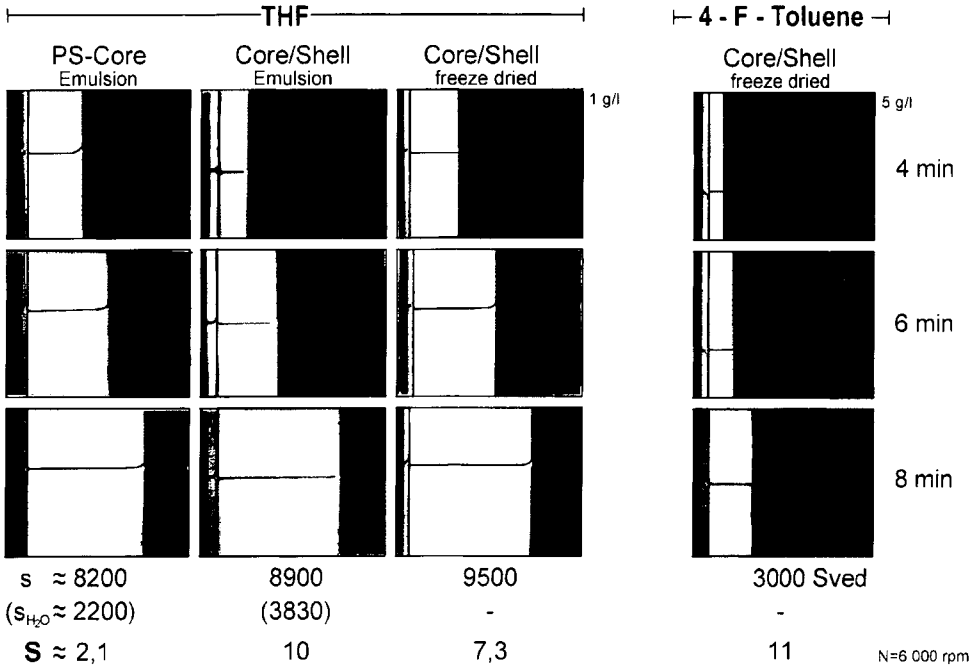

Figure 6. Schlieren photos of four sedimentation runs of two SK-26 PS/PTBA core−shell samples (from diluting the aqueous dispersion and by dissolving the freeze-dried form) in THF and 4-FT (concentration 1 and 5 g/L).

values of the slowest particles in Figure 6. According to the equation (cf. ref 39)

$$S = \left(\frac{\rho_p - \rho_{sol}}{\rho_p - \rho_{H_2O}} \frac{\eta_{H_2O}}{\eta_{sol}} \frac{s_{H_2O}}{s_{sol}}\right)^3 \qquad (3)$$

where ρ_p = particle density, unswollen in H_2O, and ρ_{sol} and η_{sol} = density and viscosity of the "solvents" H_2O, THF, and 4-FT, these $s_{50\%}$ values yield the four swelling degrees: $S = 2.1$ (core, THF), 10/7.3 (core−shell, THF), and 11 (core−shell, 4-FT). The degree of swelling of the PS core particle in THF ($S = 2.1$) agrees again very well with the known value for 1:10 cross-linked PS latex ($S = 2.2$ [30]). The overall volume swelling determined for the core−shell particles ($S \approx 7-10$), however, is considerably higher than the corresponding value obtained from light scattering, $S \approx 5$ (cf. Table 1, $R_{H,aq\ dispersion} = 170$ nm, $R_{H,THF} = 298$ nm). The difference between the AUC values obtained in THF via different sample preparations (dilution from aqueous dispersion; redispersion of freeze-dried powder) could be taken as a rough estimate of the intrinsic error of the method. However, the fact that the swelling ratio of the pure PS seeds is well reproduced might indicate that the uncertainty is connected with the swelling ratio of the shell. Following the same strategy as for the light scattering data (cf. section 3.2), one finds $S \approx 10-15$ for the PTBA shell alone, which is much higher than the values obtained for pure 1:10 cross-linked PTBA particles and higher than the corresponding light scattering result $S \approx 6-8$. This discrepancy cannot be simply due to experimental error, as similar comparisons between light scattering data and AUC results for pure cross-linked polyacrylate latex yield quite comparable swelling ratios.[39] One possible explanation is that some of the assumptions made in the derivation of eq 3 do not hold for core−shell particles.

The four relative PSD curves in organic solvents (see Figure 5b) are, as in the case of aqueous dispersions, unimodal, very narrow, and nearly monodisperse. While the absolute values of the particle diameter D are in error, the broadness parameters $(D_{90\%} - D_{10\%})/D_{50\%} = 0.12/0.11/0.07$, and 0.11 are nevertheless correct. They are very small and almost the same (i.e., homogeneous) as in H_2O. This important AUC result implies, first, the distribution of cross-linker is statistical in these core−shell particles and, second, the degree of cross-linking and therefore the degree of swelling is very uniform, regarding different particles.

3.4. Solid-State NMR Experiments. NMR spin diffusion experiments allow the characterization of heterogeneities on the length scale of one monomer unit up to 150 nm.[25] In contrast to the experiments described above, this method is suitable to give detailed information on the internal architecture of a given sample. A typical ^1H spin diffusion experiment consists of three steps: (i) the selection of proton magnetization of one component by a suitable so-called dipolar filter, (ii) ^1H spin diffusion, and (iii) the detection of the resulting distribution of proton magnetization.

The dipolar filter selects regions with differences in mobility of the polymer components whereby the mobility of polymers is related to their respective T_g. At a temperature below T_g the polymer is rigid according to very slow motions of the polymer chains. At temperatures above its T_g, the polymer is mobile. The dipolar filter that is based on the multiple pulse homonuclear decoupling[25] selects the mobile component, and the magnetization transfer takes place from the mobile to the rigid component. Although in principle this pulse sequence is capable of averaging the dipolar coupling, here it is applied in such a way that only weak dipolar couplings are averaged and the corresponding signals are retained, whereas strong dipolar couplings lead to an irreversible decay.

If there are two polymers with an ideal phase separation, only two different components in mobility are found. In the case of a mobility gradient between the phases, dipolar couplings also exhibit a gradual change between the values of the pure phases. Therefore, they

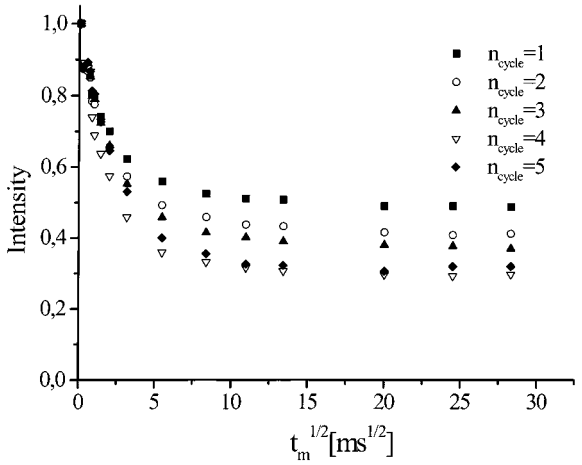

Figure 7. Results of ^{1}H spin diffusion with ^{1}H detection of the latex SK-27 (PTBA/PS inverse core−shell) shown with varying filter strength $n_{cycle} = 1-5$.

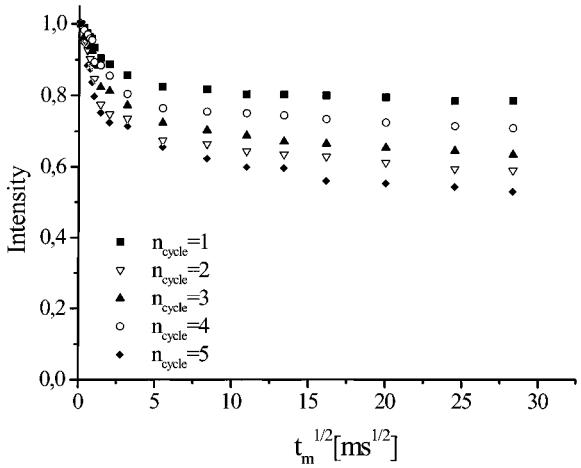

Figure 8. Results of ^{1}H spin diffusion with ^{1}H detection of the latex SK-26 (PS/PTBA core−shell) shown with varying filter strength $n_{cycle} = 1-5$.

can be distinguished with different filter strengths. Without any filter the whole particle is detected. With increasing filter strength regions with different mobilities can be selected. The strength of the filter was increased by increasing the number of cycles n_{cycle} whereas the delay time t_d was kept constant at 10 μs. After one filter cycle most of the magnetization of the rigid cross-link points with strong dipolar couplings is suppressed. Since the mobility of the surrounding (pure) component is reduced in the "interface" between the cross-link points and the other mobile units, this part is also reduced by the dipolar filter. In reverse, the mobilized portion of rigid components immersed in the core is still detected after applying a weak filter (e.g., $n_{cycle} = 1$). Because the particle size in these experiments is as large as 400 nm, the spin diffusion technique is not sensitive to the entire structure.[27] However, in the case of the PTBA/PS latexes, spin diffusion data provide a sensitive measure of the thickness and the structure of the interface.[42,43]

In Figure 7 the results of the ^{1}H spin diffusion with ^{1}H detection of the latex SK-27 with a PTBA core and PS shell are shown for varying filter strength. An increased temperature of 60 °C was required to induce a mobility to the PTBA phase according to its T_g of 40 °C, whereas PS with a T_g of 108 °C represents the rigid component (T_g data correspond to the un-cross-linked polymers). The dipolar filter suppresses the magnetization of the cross-linked PS and detects the magnetization of the PTBA. The number of filter cycles is varied between 1 and 5. The initial value is always normalized to 1.0. The signal decay occurs in two steps, indicating a superposition of two different structures. At short mixing times t_m, the magnetization of the PTBA magnetization decreases quickly, indicating a large contact area between PTBA and PS and therefore small domains in the interface between the two phases. At longer mixing times the second decay of PTBA magnetization is slower due to the detection of the entire core−shell structure of the system. With increasing filter strength the first decay becomes faster and the final value decreases, indicating a interfacial region between the components. The final value of spin diffusion curves corresponds to the amount of mobile component selected in the experiment. After the weakest filter $n_{cycle} = 1$ a fraction of 49% for the SK-27 latex is observed as would be expected from the mass ratio of the two polymers PTBA and PS. With increasing filter strength, the final value in the spin diffusion experiment becomes lower, reaching 32% for $n_{cycle} = 5$ because magnetization of immobilized PTBA in the interface is also suppressed. The ratio of immobilized PTBA to mobile PTBA is about 0.36. The fast decay at short mixing times was numerically simulated[25,26] and indicates a thickness of the interface region of about 10 nm.

The ^{1}H spin diffusion was again carried out with varying filter strength for the SK-26 with a core of PS and a shell of PTBA (Figure 8). For this particle a decay in two steps was detected. The final value of the curve using $n_{cycle} = 5$ is 53% and corresponds to the mass ratio of the polymers. The very fast decay at short mixing times and especially the high final value signals a thin interfacial region between the components of less than 5 nm. However, the magnetization decay for this latex is slower than that for the latex SK-27, indicating that the interface observed by spin diffusion can be explained by the different material diffusion lengths of the oligomers during synthesis.

4. Discussion

The main motivation of the reported work was to synthesize core−shell microgel colloids that can be used as tracer colloids to study single-particle dynamics in host dispersions of either pure polystyrene (PS; cross-linked with diisopropenylbenzene, DIPB) or pure poly(*tert*-butyl acrylate) (PTBA; cross-linked with ethylene glycol diacrylate, EGDA) particles with nearly hard-sphere-like interactions. Achieving this goal required finding the optimal reaction conditions for a two-stage surfactant-free aqueous dispersion polymerization process under the simultaneous restrictions of preventing secondary nucleation, controlling morphology to provide true core−shell structured particles, and at the same time guaranteeing very narrow size distributions for both core and shell. The quasi core−shell particles (SK-25; core PTBA/EGDA 10:1, shell PTBA/EGDA 5:1) were synthesized as a precursor to the preparation of PTBA/PS core−shell tracer particles (see below) and were later on used as host dispersion.[29] Thus they were reported here for later reference, but will not be discussed with respect to strategies of two-stage latex synthesis.

A number of different methods have been reported for preparing core−shell type particles,[44] using either reaction processes (like "seeded growth") or second-stage

polymer that favor the wanted morphology while at the same time avoiding secondary nucleation. However,[47] morphological control is difficult to achieve, when the choice of the polymer is dictated rather by optical properties than by thermodynamic affinities and reaction rates.[17,18,44]

The strategy used in this work to prepare core−shell latexes was to apply reaction conditions that are between "seeded growth" (requiring high seed latex number densities due to the low capture efficiency of second-stage polymer) and "shot addition" (increasing capture efficiency by adding the second-stage polymer before 100% conversion of the seed latex).[44] The seed latexes are polymerized to 100% conversion, but are swollen with the *second-stage monomer* in order to increase the capture efficiency and prevent secondary nucleation. In addition, starved conditions are maintained while adding the main amount of the second-stage monomer.

In the case of the polystyrene (PS) core−poly(*tert*-butyl acrylate) (PTBA) shell particles (SK-26) the morphology of the formed particle is controlled by the thermodynamic stability of the product. The structure with the lowest interfacial energies at the phase boundaries of the polymer/polymer and the polymer /water interfaces was formed, just as for un-cross-linked phase separated systems, with the more hydrophilic polymer building the shell.

By use of a variety of characterization techniques, it has been possible to verify the core−shell morphology and to draw a consistent and detailed picture of the particle structure. From the transmission electron micrographs one obtains evidence for a core−shell structure with a sharp and well-defined interface—no domains of the shell material are visible in the core. From light scattering and analytical ultracentrifuge (AUC) measurements the particle sizes of the seeds as well as of the core−shell particles in aqueous dispersion and in good solvents were determined. Together with light scattering experiments yielding the size of the swollen cores in the core−shell particles (by index matching the shells), values for the swelling ratios of both core and shell could be derived separately. We find that the swelling behavior is identical with that determined or known for the corresponding homogeneous particles. This again indicates a fully phase-separated core−shell morphology with a sharp interface.

From density gradient experiments with the AUC one finds that the two-stage latexes are of uniform chemical composition; i.e., the volume ratio of core and shell is narrowly distributed. This in turn indicates that the polydispersities of both core radius and shell thickness must be small as well, yielding a narrow size distribution for the overall particle size in accordance with the light scattering results. From AUC measurements in good solvents one, furthermore, learns that the particles are fully cross-linked, as no dissolved macromolecules were detected, and that the particles swell homogeneously, as the PSD polydispersity does not increase on dissolution (=swelling). Finally, the use of the NMR spin diffusion technique verifies that the interface is rather narrow, as expected for a thermodynamically stable structure, yielding an interface of less than 5 nm thickness.

To prepare the (thermodynamically unstable) inverse core−shell morphology with the more hydrophobic PS forming a shell around a core of the more hydrophilic PTBA (SK-27), one has to prevent the system from returning to the thermodynamically stable core−shell structure via core−shell inversion. This was achieved via kinetic stabilization of the unstable structure, i.e., by blocking polymer diffusion through cross-linking of both core and shell material. Sundberg et al.[45] have argued that cross-linking the seed introduces an additional contribution to the total free energy G determining the ultimate particle morphology which is usually determined by the interfacial free energy: the elastic free energy which takes into account the restoring forces of the network due to a displacement from the equilibrium configuration. Their calculations show that a small degree of cross-linking is sufficient to make the elastic term significantly large as compared to the interfacial term. They predict that increases in seed particle size, degree of cross-linking, and swelling ratio (of seed latex with second-stage monomer) favor inverse core−shell structures, even though the interfacial forces would have lead to core−shell inversion. Following their considerations, the PTBA seed latex (cross-linked 1:50 with EGDA) was provided with a thin shell of extremely high cross-linked (1:5) homopolymer using the same conditions as before (monomer swelling; starved conditions). Then, the second-stage polymer PS/DIPB was added under conditions that further minimize monomer or polymer diffusion into the seed: the second-stage monomer mixture was added under starved conditions only after the reaction vessel was charged with new initiator.

That this strategy was extremely successful is documented by the TEM pictures (Figure 1e,f). A pronounced core−shell structure with a well-defined interface and without domain structures results while simultaneously achieving a very narrow size distribution. That the resulting structure is unfavorable in the thermodynamic sense is indicated by the fact that even though polymer diffusion was strongly hindered, the resulting interfacial region is significantly larger as in case of the PS/PTBA particles. From the NMR spin diffusion experiments an interfacial thickness of 10 nm is estimated.

These results are also supported by the light scattering experiments, even though an anomalously high swelling ratio was found for the PS shell. However, this may partly be due to the use of an homogeneous particle model in order to analyze the data. Alternatively, this could indicate that the outer shell is not completely closed or that the cross-link distribution in the shell is inhomogeneous. A final answer to this question has to be deferred to a more refined analysis of the particle form factor with a more realistic core−shell model and further experiments where the shell thickness is varied systematically. Nevertheless, it could be demonstrated that a high cross-linking density of seed latex and shell polymer efficiently stabilize thermodynamically unstable core−shell structures.

5. Conclusion

The synthesis of phase-separated core−shell and inverse core−shell structured particles using styrene and *tert*-butyl acrylate as monomers have been reported. The reaction conditions were optimized in order to take the thermodynamic stability of the resulting morphology into account. For the polystyrene (PS; cross-linked with diisopropenylbenzene)/poly-(*tert*-butyl acrylate) (PTBA; cross-linked with ethylene glycol diacrylate) core−shell structure reaction conditions between "seeded growth" and "shot addition" lead to a well-defined, phase-

separated structure. The thermodynamic stability of this morphology leads to a very thin (<5 nm) interfacial region between the two phases and no domains were detected by solid-state NMR. The core−shell structure was analyzed in detail by combining TEM, light scattering, analytical ultracentrifuge (AUC) measurements, and NMR spin diffusion. The chemical homogeneity and the stability of the swollen particle was shown by AUC measurements. No linear polymer is dissolved; thus the core−shell particles are completely cross-linked. To synthesize the thermodynamically unfavorable PTBA/PS inverse core−shell structure, we made use of the concept of kinetic stabilization by preventing core−shell inversion through synthesis of a very highly cross-linked intermediate layer that separates a moderately cross-linked PTBA core from a highly cross-linked PS shell. As expected for this structure the interfacial region is increased up to 10 nm, but no domain structures can be detected. The core−shell particles will be used in future work as tracer colloids to study single-particle dynamics in highly concentrated dispersions.

Acknowledgment. S.K. thanks V. Frenz for his helpful discussions to find polymer components suitable for preparing a host-tracer system of microgels for light scattering experiments. Furthermore, financial support by SFB 262 is also gratefully acknowledged. We thank Dr. G. Lieser and G. Weber for their help in the electron microscopic investigations.

References and Notes

(1) Eliseeva, V. I. *Prog. Org. Coatings* **1985**, *13*, 195.
(2) Devon, M.; Gardon, J.; Roberts, G.; Rudin, A. *J. Appl. Polym. Sci.* **1990**, *39*, 2119.
(3) Blankenship, R.; Kowalski, A. U.S. Patent **1986**, 4,594,363 (June 10).
(4) Silverstein, M.; Talmon, Y.; Narkis, M. *Polymer* **1989**, *30*, 416.
(5) van Megen, W.; Pusey, P. N. *Phys. Rev.* **1991,** *A43*, 5429.
(6) van Megen, W.; Underwood, S. M. *Phys. Rev.* **1994**, *E49*, 4206.
(7) Bartsch, E.; Frenz, V.; Moeller, S.; Sillescu, H. *Physica* **1993**, *A201*, 363.
(8) Bartsch, E.; Frenz, V.; Baschnagel, J.; Schaertl, W.; Sillescu, H. *J. Chem. Phys.* **1997**, *106*, 3743.
(9) Goetze, W. In *Liquids, Freezing and the Glass Transition*, Les Houches, Session LI; Levesque, D., Hansen, J. P., Zinn-Justin, J., Eds.; Elsevier: Amsterdam, 1990.
(10) Goetze, W.; Sjoegren, L. *Rep. Prog. Phys.* **1992**, *55*, 241.
(11) Pecora, R. *Dynamic Light Scattering*, Plenum: New York, 1985.
(12) Kasper, A.; Kirsch, S.; Renth, F.; Bartsch, E.; Sillescu, H. *Prog. Colloid Polym. Sci.* **1996**, *100*, 151.
(13) Renth, F.; Bartsch, E.; Kasper, A.; Kirsch, S.; Stoelken, S.; Sillescu, H.; Koehler, W.; Schaefer, R. *Prog. Colloid Polym. Sci.* **1996**, *100*, 127.
(14) Okubo, M.; Katsuta, Y.; Matsumoto, T. *J. Polym. Sci., Polym. Lett. Ed.* **1980**, *18*, 481.
(15) Muroi, S.; Hashimoto, H.; Hosoi, K. *J. Polym. Sci., Polym. Chem. Ed.* **1984**, *22*, 1365.
(16) Okubo, M.; Katsuta, Y.; Matsumoto, T. *J. Polym. Sci., Polym. Chem. Ed.* **1980**, *16*, 3219.
(17) Lee, D. I.; Ishikawa, T. *J. Polym. Sci., Polym. Chem. Ed.* **1983**, *21*, 147.
(18) Lee, S.; Rudin, A. *J. Polym. Sci.* **1992**, *A30*, 865.
(19) Schmitz, K. S. *An Introduction to Dynamic Light Scattering by Macromolecules*; Academic Press: San Diego, 1990.
(20) Pusey, P. N.; van Megen, W. *J. Chem. Phys.* **1984**, *80*, 3513.
(21) Maechtle, W. In *Analytical Ultracentrifugation in Biochemistry and Polymer Science*; Harding, S. E., et al. Eds.; Royal Society of Chemistry: Cambridge, 1992; Chapter 10.
(22) Grunder, R.; Kim, Y. S.; Ballauff, M. *Angew. Chem.* **1991**, *103*, 1715.
(23) Beyer, D.; Lebek, W.; Hergeth, W.-D.; Schmutzler, K. *Colloid Polym. Sci.* **1990**, *268*, 744.
(24) Milles, M. F.; Gilbert, R. G.; Napper, D. H.; Rennie, A. R.; Ottewill, R. H. *Macromolecules* **1993**, *26*, 3553.
(25) Schmidt-Rohr, K.; Spiess, H. W. In *Multidimensional Solid-State NMR and Polymers*; Academic Press: London, 1994.
(26) Spiegel, S. Ph.D. Thesis, Mainz, 1995.
(27) Landfester, K.; Boeffel, C.; Lambla, M.; Spiess, H. W. *Macromol. Symp.* **1995**, *92*, 109.
(28) Landfester, K.; Boeffel, C.; Lambla, M.; Spiess, H. W. *Macromolecules* **1996**, *29*, 5972.
(29) Kirsch, S.; Bartsch, E.; Sillescu, H. Manuscript in preparation.
(30) Kirsch, S. Doerk, A.; Bartsch, E.; Sillescu, H.; Landfester, K.; Spiess, H.-W.; Maechtle, W. Submitted for publication.
(31) Kotera, A.; Furusawa, F.; Takeda, Y. *Kolloidz. Z. Polym.* **1970**, *39*, 677.
(32) Koppel, D. E. *J. Chem. Phys.* **1972**, *57*, 4814.
(33) Brown, W., Ed. *Dynamic Light Scattering*; Clarendon: Oxford, 1993.
(34) Maechtle, W.; Klodwig, U. *Macromol. Chem.* **1979**, *180*, 2507.
(35) Maechtle, W. *Macromol. Chem. Macromol. Symp.* **1992**, *61*, 131.
(36) Here R_H measured in THF was used instead of the value measured in 4-FT since the DLS results can be interpreted by applying the homogeneous particle relationship (eq 2) in the first approximation. With 4-FT the core−shell nature of SK-26 would have to be taken into account explicitly by solving the integral (2) using a $P(qR)$ with a nearly index-matched shell. This could not yet be done. Analyzing DLS data in 4-FT in the homogeneous sphere approximation yields $R_H = 272$ nm (cf. Table 1) which significantly underestimates the actual size and leads to a swelling ratio for the shell which is too small.
(37) Kerker, M. *The Scattering of Light and Other Electromagnetic Radiation*; Academic Press: New York, 1969.
(38) Maechtle, W. *Angew. Makromol. Chem.* **1988**, *162*, 35.
(39) Maechtle, W.; Ley, G.; Streib, J. *Prog. Colloid Polym. Sci.* **1995**, *99*, 144.
(40) It should be noted that the apparent tailing of the PSD toward larger particle sizes is due to instrumental resolution effects originating from the finite size of the detector slit and the low signal intensities at the front edge of the sedimentation front (containing the largest particles).
(41) The fact that the turbidity bands appear to be broadened as compared to the ones in aqueous dispersion does not imply a corresponding broadening of the PSD. Due to solvent uptake (swelling) in good solvents, the refractive index difference between particles and medium is reduced, leading to lower scattering intensities. This had to be compensated by increasing the particle concentration by a factor of 5. This and the particle size increase due to swelling lead to an intrinsic broadening of the turbidity bands or, loosely speaking, to a broadening of the instrumental resolution function.
(42) Spiegel, S.; Landfester, K.; Lieser, G.; Boeffel, C.; Spiess, H. W.; Eidam, N. *Macromol. Chem. Phys.* **1995**, *196*, 985.
(43) Landfester, K., Spiess, H. W. *Acta Polym.* **1998**, *49*, 451.
(44) Chainey, M.; Hearn, J.; Wilkinson, M. C. *Br. Polym. J.* **1981**, 15, 132.
(45) Sundberg, D. C.; Durand, Y. G. *Macromol. Symp.* **1995**, *92*, 43.

MA980916E